

NASA TECHNICAL NOTE



NASA TN D-2470

c 1

LOAN COPY: RI
AFWL (WL
KIRTLAND AFB

0079601



TECH LIBRARY KAFB, NM

NASA TN D-2470

EXPERIMENTAL EVALUATION OF SIZE EFFECTS ON STEADY-STATE CONTROL PROPERTIES OF ELECTRON-BOMBARDMENT ION THRUSTOR

by Eugene V. Pawlik and Shigeo Nakanishi

Lewis Research Center

Cleveland, Ohio



0079601

EXPERIMENTAL EVALUATION OF SIZE EFFECTS ON STEADY-
STATE CONTROL PROPERTIES OF ELECTRON-
BOMBARDMENT ION THRUSTOR

By Eugene V. Pawlik and Shigeo Nakanishi

Lewis Research Center
Cleveland, Ohio

NATIONAL AERONAUTICS AND SPACE ADMINISTRATION

For sale by the Office of Technical Services, Department of Commerce,
Washington, D.C. 20230 -- Price \$0.75

EXPERIMENTAL EVALUATION OF SIZE EFFECTS ON STEADY-
STATE CONTROL PROPERTIES OF ELECTRON-
BOMBARDMENT ION THRUSTOR

by Eugene V. Pawlik and Shigeo Nakanishi

Lewis Research Center

SUMMARY

The steady-state gains (variations of beam current with changes in thruster input variables) were determined experimentally for a range of electron-bombardment ion thruster diameters. Thruster operation was compared for 5-, 10-, and 20-centimeter-diameter exhaust beam sources, primarily at a specific impulse of 4000 seconds, with mercury as the propellant. The steady-state gains with respect to each thruster input variable are presented for each thruster size. The effects of thruster size on the control properties or gains of the ion thruster were slight except for the smallest unit. For this case, propellant flow gains were higher than for the other sizes, and a quenching of the plasma was noticeable at low flows.

Thruster operation of a 10-centimeter-diameter unit was also investigated with an alkali earth coated filament. The steady-state gains of this filament were time variant during the initial operating period.

INTRODUCTION

Electron-bombardment ion thrusters have been extensively investigated (e.g., refs. 1 to 3) and are at a state of development where typical thruster characteristics or functional relations between thruster output and the input variables can be obtained for use in propulsion-system design studies. The steady-state gains or variations in ion beam current with changes in input variables are useful parameters in control system design (ref. 4) and have been determined experimentally for a 10-centimeter-diameter thruster (ref. 5). Since a range of thruster sizes may be required for space-flight missions, investigating scaling effects on thruster gains is of interest.

Possible applications of ion thrusters extend over a spectrum ranging from station keeping and attitude control of satellites to primary propulsion systems for interplanetary vehicles. Correspondingly, the optimum specific impulse, propellant flow rate, and thruster size may vary considerably. In the investigation of reference 6 the effects of scaling (for 5- to 20-cm-diam. sources) upon ion source performance, as determined by the ion chamber operating efficiency, were noticeable only for the smallest thruster size. The pur-

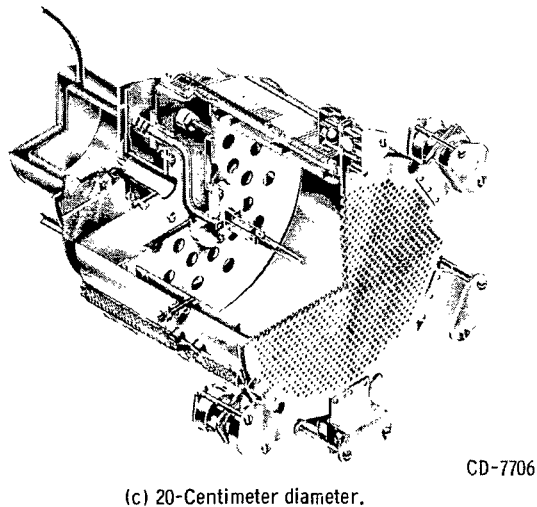
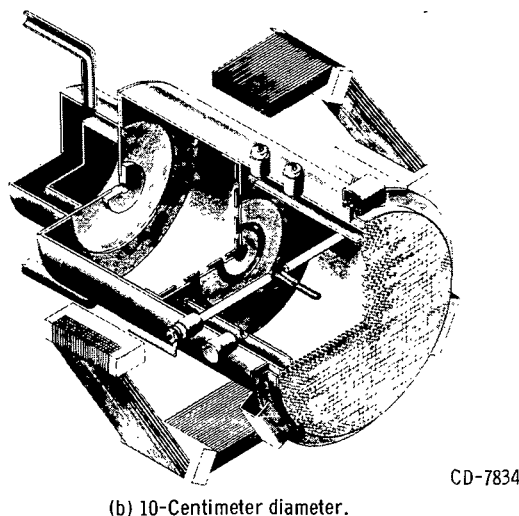
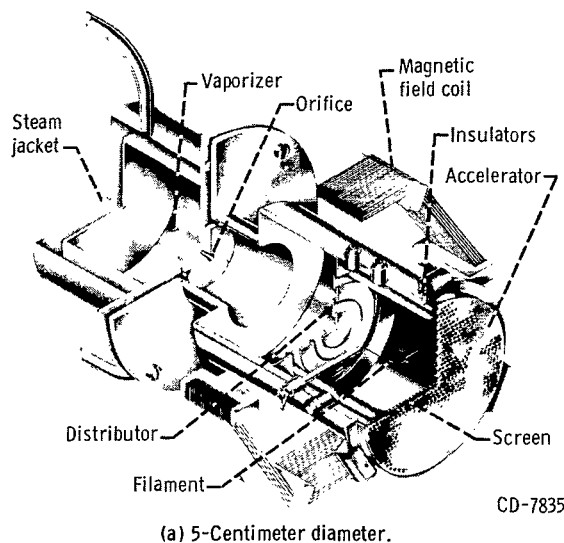


Figure 1. - Cutaway drawings of electron-bombardment ion thrusters.

pose of the present investigation was to determine whether there are significant size effects on the gains of these thrusters.

The results of these tests are compared with those of a 10-centimeter-diameter ion source previously reported in reference 5.

APPARATUS

Thrusters

The three ion thrusters compared herein produce 5-, 10-, and 20-centimeter-diameter exhaust beams. Cutaway drawings of the thrusters are shown in figure 1. The 5-centimeter thruster (fig. 1(a)) was a scaled version of the 10-centimeter size (fig. 1(b)) and differed only in the filament supports. The 20-centimeter size (fig. 1(c)) differed in distributor geometry and magnetic field shape.

Interchangeable sharp-edged orifices were used to control the propellant flow rate from the steam-heated vaporizer. A range of orifice sizes was used to obtain equivalent propellant flow rates corresponding to values from 0.029 to 1.250 amperes of singly charged mercury ions. The orifice sizes used and the average calibration flow rates are presented in the table on page 3 for a vaporizer temperature of 210.8° F. The flow rates were determined by weight losses for a long operating period with the vaporizer held at a constant temperature.

After leaving the vaporizer through the orifice, the propellant atoms flow into the ionization chamber through a flow distributor. The ion chamber contains a cylindrical anode with a length-to-diameter ratio of about 0.75. A thermionic electron emitter is located on the axis of the chamber. An axial magnetic field in-

Orifice diameter, cm	Flow rate, g/hr	Equivalent flow rate, J_N , amp	Commonly used with thruster diameter, ϕ , cm, of -
0.076	0.22	0.029	5
.093	.31	.041	5,10
.102	.46	.062	5,10
.127	.58	.078	5,10
.152	.84	.112	5,10
.183	1.21	.161	10
.206	1.52	.203	10
.254	2.33	.311	10,20
.359	4.57	.610	20
.440	7.21	.963	20
.508	9.36	1.250	20

creases the probability of collision between the emitted electrons and the mercury propellant by preventing the rapid escape of the electrons to the anode. The field windings provide a tapered field with a downstream-to-upstream magnetic-field-strength ratio of approximately 0.6 along the axis of the ion chamber. The downstream field is measured at the screen grid and the upstream field at the distributor. The magnetic field strength at the most efficient ion chamber operating point varies approximately inversely with the thruster diameter (ref. 6).

During thruster operation, the electron bombardment of the mercury propellant produces a plasma within

the ion chamber. Most of the electrons in this plasma are extracted at the anode, while the majority of the ions that diffuse to the screen at the downstream end of the chamber are accelerated to form the ion beam.

The accelerating system is composed of a pair of grids, which are designated the screen and the accelerator. These two grids are aligned and electrically insulated by aluminum oxide spheres as shown in figure 1. The spacing between the grids is determined by the diameter of the sphere used. The 0.130-centimeter-thick molybdenum grids were match drilled with 0.476-centimeter-diameter holes on 0.635-centimeter equilateral triangular hole spacing. The distance between screen and accelerator was measured at five locations before and after each run. The grid spacing was approximately 0.160 centimeter for all the data presented.

The 5-centimeter-diameter thruster employed two strands of twisted tantalum wire for a filament, whereas the 10- and 20-centimeter-diameter units normally utilized a V-shaped tantalum ribbon. The 10-centimeter-diameter thruster was operated with a barium oxide coated filament, which was wound with fine tantalum wires to provide supporting surfaces for the emissive coating.

Facility and Electrical System

The ion thrusters used in this program were mounted in a thruster compartment connected by a 26-inch gate valve to a 5-foot-diameter by 16-foot-long vacuum tank. The tank is evacuated by four 32-inch-diameter oil diffusion pumps backed up by an ejector and a mechanical pump. A cutaway view of the vacuum facility and the thruster compartment is shown in figure 2.

A liquid-nitrogen-cooled condenser is used to supplement the diffusion pumps. The condenser has an area of approximately 33 square meters and together with the diffusion pumps enables the tank to be evacuated to 2×10^{-6} torr

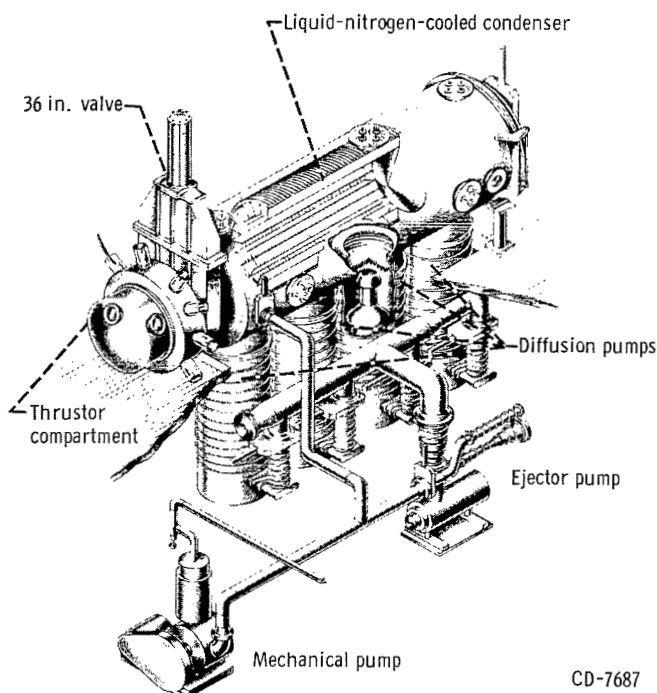


Figure 2. - Cutaway drawing of vacuum tank installation.

the desired vacuum conditions. Steam was supplied to the vaporizer to start the propellant flow and after a short waiting period (3 to 5 min) the system reached operating temperature. Voltages were then applied to the thrustor.

Magnetic-field
coil (around
thrustor)

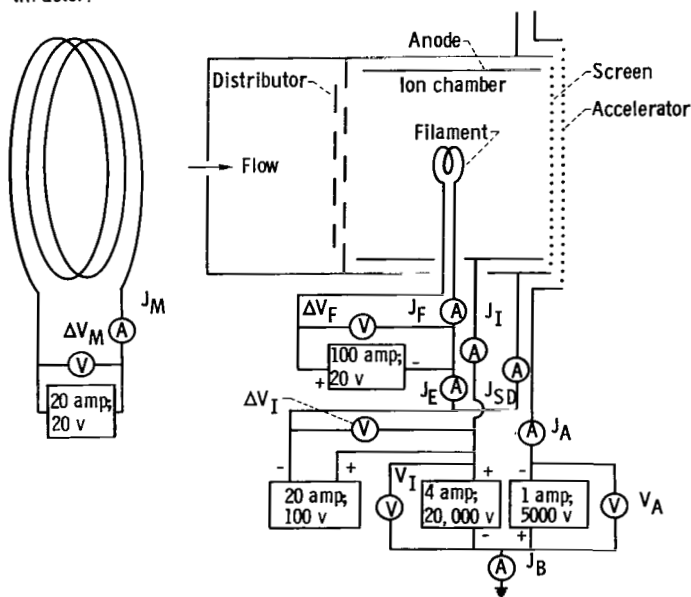


Figure 3. - Wiring diagram of ion thrustor.

and the thrustor compartment to 4×10^{-6} torr. With the 20-centimeter-diameter thrustor operating, the tank pressure rose to approximately 6×10^{-6} torr and the thrustor compartment to 1×10^{-5} torr.

Electrical power supplies and meters were connected as shown in the schematic diagram of figure 3. Standard panel meters of 3-percent accuracy were used for all electrical measurements. The same power supplies were used for operation of all three thrustor sizes. No closed-loop regulation existed in these supplies.

PROCEDURE

After the thrustor was mounted in the thrustor compartment, the tank was pumped down to

Initiating the discharge usually required raising the discharge chamber voltage to about 70 volts, but during thrustor operation the discharge chamber voltage was normally set at 50 volts. At 50 volts doubly charged ions have been shown to constitute 5 percent or less of the ion beam (ref. 7). The anode potential (or net accelerating potential) was maintained at the desired positive voltage. The screen and the distributor are physically connected to the thrustor body and consequently were at the same potential. The filament heater supply was connected to the thrustor body through the filament emission current meter. A negative voltage was applied to the accelerator to prevent electron back streaming from the tank to the thrustor. Back streaming, in addition to causing undesirable

arcing from the tank environment to the thruster, could cause the ground return meter (beam current) to read high and introduce a large error into the beam reading. Values of the ratio of net-to-total accelerating voltage R equal to or below 0.8 have been found necessary to prevent electron back streaming (ref. 5) for the accelerator grids used herein. All data presented herein were taken without a neutralizer. Normal thruster testing in a vacuum chamber does not require the neutralizer to supply electrons because the ion beam is electrically connected to the tank walls. During this operating mode, charge neutralization is accomplished by electrons supplied from the walls and to a smaller extent from the residual gas. Use of the neutralizer does not contribute significantly towards thruster operation under these conditions (e.g., see ref. 8).

The thrusters used in this study were primarily operated at conditions corresponding to near-optimum performance. Previous investigations (ref. 9) have shown that at a specific impulse of 4000 seconds a propellant utilization efficiency η_u of 80 percent is very nearly the optimum on the basis of thruster efficiency. The primary inputs to the thruster are the filament heating current J_F , the accelerator potential V_A , anode (net accelerating) potential V_I , the ion-chamber potential difference ΔV_I , the magnetic field B ($B \propto$ magnetic field current J_M), and the neutral mercury propellant flow rate J_N (measured in amp equivalent flow of Hg^+). The major output of the thruster is the beam current J_B because at a given net accelerating voltage and propellant charge-to-mass ratio the thrust is a function only of ion beam current.

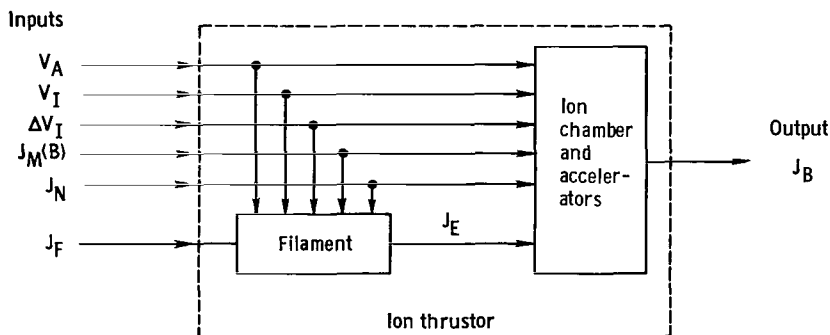


Figure 4. - Block diagram of ion thruster.

The thruster is represented in figure 4 by its two major components, the filament and the ion-chamber - accelerator system. The primary inputs that determine the beam-current output are considered to be independent variables since a change in any of the primary inputs can be made without influencing the remaining input variables. The filament emission current

J_E , which is shown as the output of the filament, can be considered a secondary input variable to the ion chamber and the accelerator. The emission current is a dependent variable and is influenced strongly by the filament heating current and to some degree by each of the remaining variables. The gain of the ion-beam current with respect to each input variable was determined by varying the input in question while maintaining the remaining inputs at constant values. Varying the loading on several of the power supplies by changing the beam current would cause a small voltage variation in the power supplies. This variation is a function of the unregulated characteristics of the supply used and was corrected for in maintaining the inputs constant. For each setting of the controlled input parameter, panel meter readings were recorded for each thruster variable. The data taken in this manner are presented for each thruster

size in table I.

The thrusters were operated at beam currents ranging from a few milliamperes to 0.090, 0.165, and 1.100 amperes for the 5-, 10-, and 20-centimeter-diameter thrusters, respectively. The thruster inputs were varied over the entire range of operational stability except for the magnetic field, which was limited by the power supply. The net accelerating potential was varied from 1000 to 4500 volts and the accelerator potential from -200 to -2000 volts. Ion-chamber potential difference was investigated over a range of 20 to 90 volts for all three thrusters. Magnetic fields of 16 to 148 gauss were used on the 5-centimeter-diameter thruster and 4 to 24 gauss on the 20-centimeter-diameter thruster. Barium oxide coated cathode data with the 10-centimeter-diameter thruster were obtained at a constant magnetic field of 30 gauss. The full range of magnetic field from 0 to 50 gauss was covered with the 10-centimeter-diameter thruster during the investigation reported in reference 5.

RESULTS AND DISCUSSION

Identification of the functional relations between input and output is one of the preliminary steps in control system design. The thruster relations or processes during steady-state operation have been identified and are reported in reference 5 for the 10-centimeter-diameter thruster. The process output of interest, the thrust, can be presented as a function of the thruster variables by the following relation:

$$F = \dot{m} \bar{v} = \frac{m}{q} J_N \eta_u \sqrt{\frac{2q}{m}} V_I = J_B \sqrt{\frac{2m}{q}} V_I \quad (1)$$

(All symbols are defined in the appendix.) Equation (1) is used with the assumption that the ion beam consists of singly charged ions and that the flow is one dimensional. The net accelerating potential V_I and the propellant flow rate J_N are directly controlled. The thrust can be represented as an explicit function of the beam current for any given setting of the net accelerating voltage. The beam current in turn can be expressed as a function of the thruster inputs. Changes in beam current can therefore be represented by the following linear relation:

$$dJ_B = \frac{\partial J_B}{\partial J_F} dJ_F + \frac{\partial J_B}{\partial V_I} dV_I + \frac{\partial J_B}{\partial V_A} dV_A + \frac{\partial J_B}{\partial (\Delta V_I)} d(\Delta V_I) + \frac{\partial J_B}{\partial J_N} dJ_N + \frac{\partial J_B}{\partial B} dB \quad (2)$$

In the prior study of control properties it was expedient to present functional relations in the form of ratios about a design point or base point of the thruster variables in order to reduce filament time variance effects and also to minimize the influence of the parameters on the emission current levels. This normalization becomes even more significant in the present study since a comparison over a wide range of beam outputs is presented. The normalized form of equation (2) that was convenient is

$$d\left(\frac{J_B}{J_{B,0}}\right) = \frac{\frac{\partial\left(\frac{J_B}{J_{B,0}}\right)}{\partial\left(\frac{J_F}{J_{F,0}}\right)} d\left(\frac{J_F}{J_{F,0}}\right) + \frac{\frac{\partial\left(\frac{J_B}{J_{B,0}}\right)}{\partial V_I} dV_I + \frac{\frac{\partial\left(\frac{J_B}{J_{B,0}}\right)}{\partial V_A} dV_A + \frac{\frac{\partial\left(\frac{J_B}{J_{B,0}}\right)}{\partial(\Delta V_I)} d(\Delta V_I)}{\frac{\partial\left(\frac{J_B}{J_{B,0}}\right)}{\partial\left(\frac{J_F}{J_{F,0}}\right)}} + \frac{1}{J_{B,0}} \frac{\partial J_B}{\partial J_N} dJ_N + \frac{\frac{\partial\left(\frac{J_B}{J_{B,0}}\right)}{\partial\left(\frac{B}{B_0}\right)} d\left(\frac{B}{B_0}\right) \quad (3)$$

The steady-state thruster gain or change in thrust level with a change in input level is represented by a partial derivative $\partial(J_B/J_{B,0})/\partial x_i$ for each input variable x_i . The thruster gains are readily obtainable by operating the thruster with all inputs constant except x_i . Deviations about an operating point may be represented to first-order accuracy by a summation of the changes in the inputs and the gains of the system:

$$\Delta\left(\frac{J_B}{J_{B,0}}\right) = K_F \Delta\left(\frac{J_F}{J_{F,0}}\right) + K_I \Delta V_I + K_A \Delta V_A + K_D \Delta(\Delta V_I) + \frac{K_N}{J_{B,0}} (\Delta J_N) + K_M \Delta\left(\frac{B}{B_0}\right) \quad (4)$$

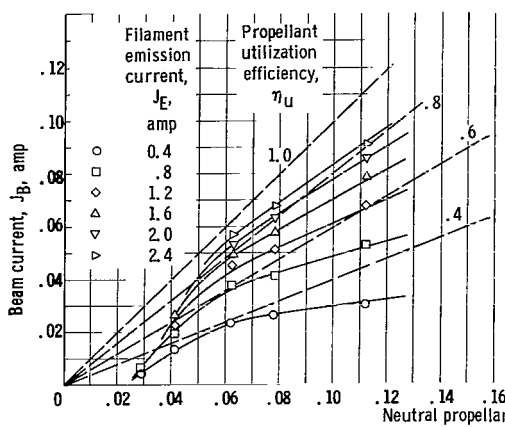
This linear relation is valid only for small excursions in the input variables. It would also be expected to hold over a range of thruster diameters provided that nonlinear effects did not arise because of thruster size.

In the discussion that follows, the variations in ion beam current with the input parameter changes are examined in the following order: neutral propellant flow rate J_N , filament heating current J_F , filament emission current J_E , anode potential V_I , accelerator potential V_A , ion-chamber potential difference or discharge voltage ΔV_I , and magnetic field intensity B . The discussions on filament heating current, filament emission current, and discharge voltage include data for a 10-centimeter-diameter thruster that utilized a barium oxide coated filament as well as the refractory metal filament normally used.

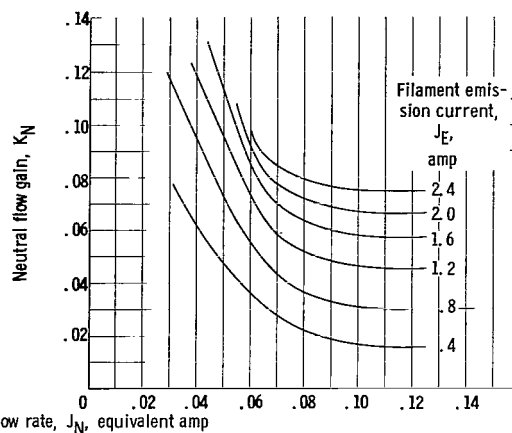
Most thruster operation was compared at an anode voltage of 2500 volts. With mercury as the propellant this voltage corresponds to a specific impulse of about 4000 seconds as determined by the equation $I = \eta_u(\bar{v}/g)$.

Thruster diameter, ϕ , cm	Magnetic field at screen, B_0 , gauss
5	56
10	30
20	16

Each thruster size was operated at a magnetic field strength that minimized ion-chamber discharge losses. These values of magnetic field strength were used as base point levels for each module size and are tabulated as shown in the table at the left.

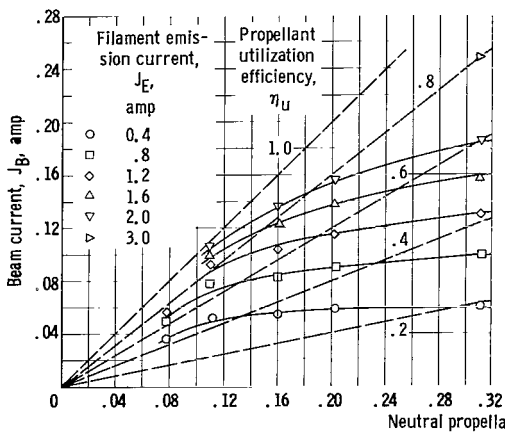


(a) Beam current as function of neutral propellant flow rate for six values of filament emission current.

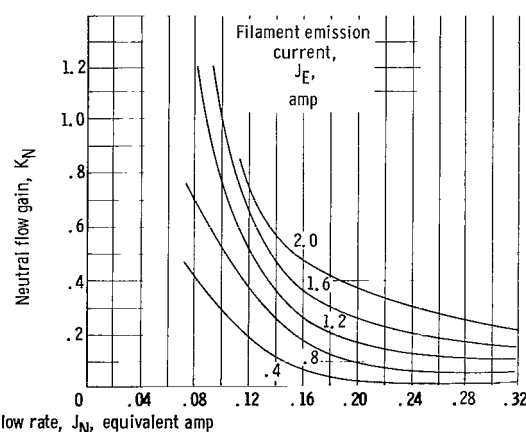


(b) Beam current to propellant flow gain as function of propellant flow rate.

Figure 5. - Ion-beam-propellant flow characteristics for 5-centimeter-diameter thruster. Anode potential, 2500 volts; accelerator potential, -625 volts; ion-chamber potential difference, 50 volts; magnetic field, 56 gauss.

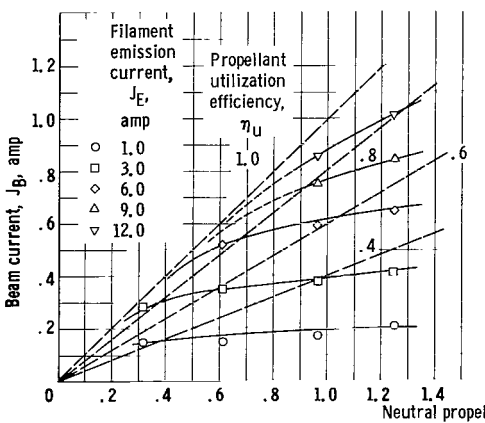


(a) Beam current as function of neutral propellant flow rate for six values of filament emission current.

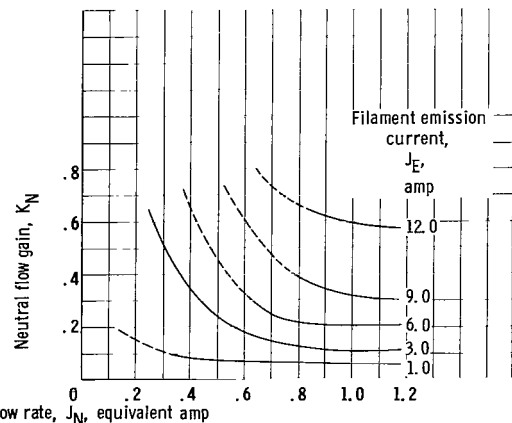


(b) Beam current to propellant flow gain as function of propellant flow rate.

Figure 6. - Ion-beam-propellant flow characteristics for 10-centimeter-diameter thruster. Anode potential, 2500 volts; accelerator potential, -625 volts; ion-chamber potential difference, 50 volts; magnetic field, 30 gauss.



(a) Beam current as function of neutral propellant flow rate for five values of filament emission current.



(b) Beam current to propellant flow gain as function of propellant flow rate.

Figure 7. - Ion-beam-propellant flow characteristics for 20-centimeter-diameter thruster. Anode potential, 4000 volts; accelerator potential, -1000 volts; ion-chamber potential difference, 50 volts; magnetic field, 16 gauss.

Neutral Flow

The 5- and the 20-centimeter-diameter thrusters were both operated over a range of neutral propellant flow rates and compared with similar data for the 10-centimeter-diameter thruster of reference 5. Orifice sizes corresponding to a flow rate ranging from 0.029 to 0.112 ampere of singly charged mercury ions were used with the 5-centimeter-diameter unit. These data are presented in table I(a). Cross plots of beam current against filament emission current from table I(a) were used to obtain the plots of ion-beam current as a function of neutral propellant flow. These curves are presented in figure 5(a) for an anode voltage of 2500 volts. The emission current J_E is used as a parameter to compare the dependence of beam current on ion-chamber performance. Dashed lines are drawn on the figure to indicate curves of constant propellant utilization efficiency. The magnetic field and discharge voltage were maintained at 56 gauss and 50 volts, respectively. The neutral propellant flow gain K_N is shown in figure 5(b) for the same values of filament emission current as shown in figure 5(a). The gains are essentially the derivatives at any point of the beam-current - neutral-flow curves of figure 5(a). The derivatives were obtained graphically and were plotted as points through which a smooth and continuous curve was faired.

The 10-centimeter-diameter thruster had been previously investigated for variations in beam current with neutral flow. This information, contained in reference 5, is reproduced herein in figure 6. Data for orifice sizes corresponding to flow rates of 0.078 to 0.311 ampere are plotted in figure 6(a). The steady-state gains K_N are shown in figure 6(b) for several values of constant filament emission current. The magnetic field was maintained at 30 gauss and the discharge voltage at 50 volts.

Variations in beam current with neutral flow were obtained for the 20-centimeter-diameter thruster for flow rates corresponding to 0.311 to 1.250 amperes. These data are tabulated in table I(c) and are plotted in figure 7(a) for a net accelerating potential of 4000 volts. Figure 7(b) shows the corresponding gains K_N again for several values of constant emission current. The magnetic field was maintained at 25 gauss and the discharge voltage at 50 volts. The 20-centimeter data were obtained at a higher anode voltage in order to maintain low accelerator impingement currents (see fig. 6 in ref. 3). The effect of this higher voltage was to displace the curves of beam current against neutral flow about 10 percent above those obtained at an anode voltage of 2500 volts.

As shown in figure 5(a) (5-cm-diam. thruster), at a constant value of filament emission current, beam current output tends to drop rapidly at low levels of neutral propellant flow rate. Thruster operation at neutral flows equivalent to 0.02 ampere of singly ionized mercury or lower could not be achieved. The beam current dropoff occurs at flow rates just below the flow rate that yields the maximum propellant utilization efficiency for each curve of constant emission current. This output dropoff was also noted for the 10-centimeter-diameter unit but was not apparent for the 20-centimeter-diameter thruster for the range of neutral flows considered (fig. 7(a)). Thruster efficiency decreased rapidly for values of neutral flows within the dropoff region

because of an increase in ion chamber losses. The energy losses involved in the ionization process are calculated by multiplying the ion-chamber potential difference ΔV_I by the difference between the anode and the beam currents. When this product is divided by the beam current, the quotient represents the energy dissipated in the ion chamber per beam ion \mathcal{E} . As shown in reference 6 the ion-chamber losses are much higher in the 5-centimeter-diameter thruster than in the two larger units. The radial potential drop within the chamber is felt to be responsible for a greater portion of the ion-chamber power being used for ohmic heating of the plasma as the thruster size decreases. The expression for this radial potential variation is (ref. 10)

$$\Delta V_r = \frac{10^{11} J_- \bar{V}_-^{1/2}}{l \pi L_c^2 \eta_-^2 \sigma_E} \quad (5)$$

If it is assumed that the electron current J_- is proportional to the emission current and that the mean thermal potential of the electrons \bar{V}_- does not change greatly, a decrease in neutral propellant flow rate at constant filament emission current would change the numerator of equation (5) but slightly.

The number density of electrons η_- (or ions in a macroscopically neutral plasma), on the other hand, would be expected to decrease in proportion to the neutral propellant flow rate. In equation (5) the radial potential drop increases inversely as the square of the number density. The ion-chamber losses due to ohmic heating of the plasma associated with the radial potential drop can thus be expected to rise rapidly with decreasing propellant flow rate, particularly in the presence of a higher magnetic field intensity (or smaller electron cyclotron radius L_c) as is the case in the small-diameter thruster.

The neutral flow gain for various values of emission current for the 5-, 10-, and 20-centimeter-diameter thruster sizes as shown in figures 5(b), 6(b), and 7(b) decreased rapidly to a minimum value as the propellant flow was increased. The gains increased as emission current was increased. The value of flow rate J_N at which the beam current dropoff occurred appeared to be proportional to thruster diameter for a filament emission current of 1 ampere. The gains at high neutral flow rates for the 10- and 20-centimeter-diameter thrusters were comparable at low values of filament emission current (below 3 amp). The gains of the 5-centimeter-diameter thruster reached minimum levels that were of the order of five times higher than those of the larger units at comparable values of filament emission current.

For all subsequent discussions, the neutral propellant flow rate was held constant at a value above the dropoff region (in a region of constant gain) when the other inputs to the thrusters were investigated.

Filament Heating Current

A plot of beam current over a range of filament heating current inputs for an anode voltage of 2500 volts is shown in figure 8(a) for the 5- and the 20-

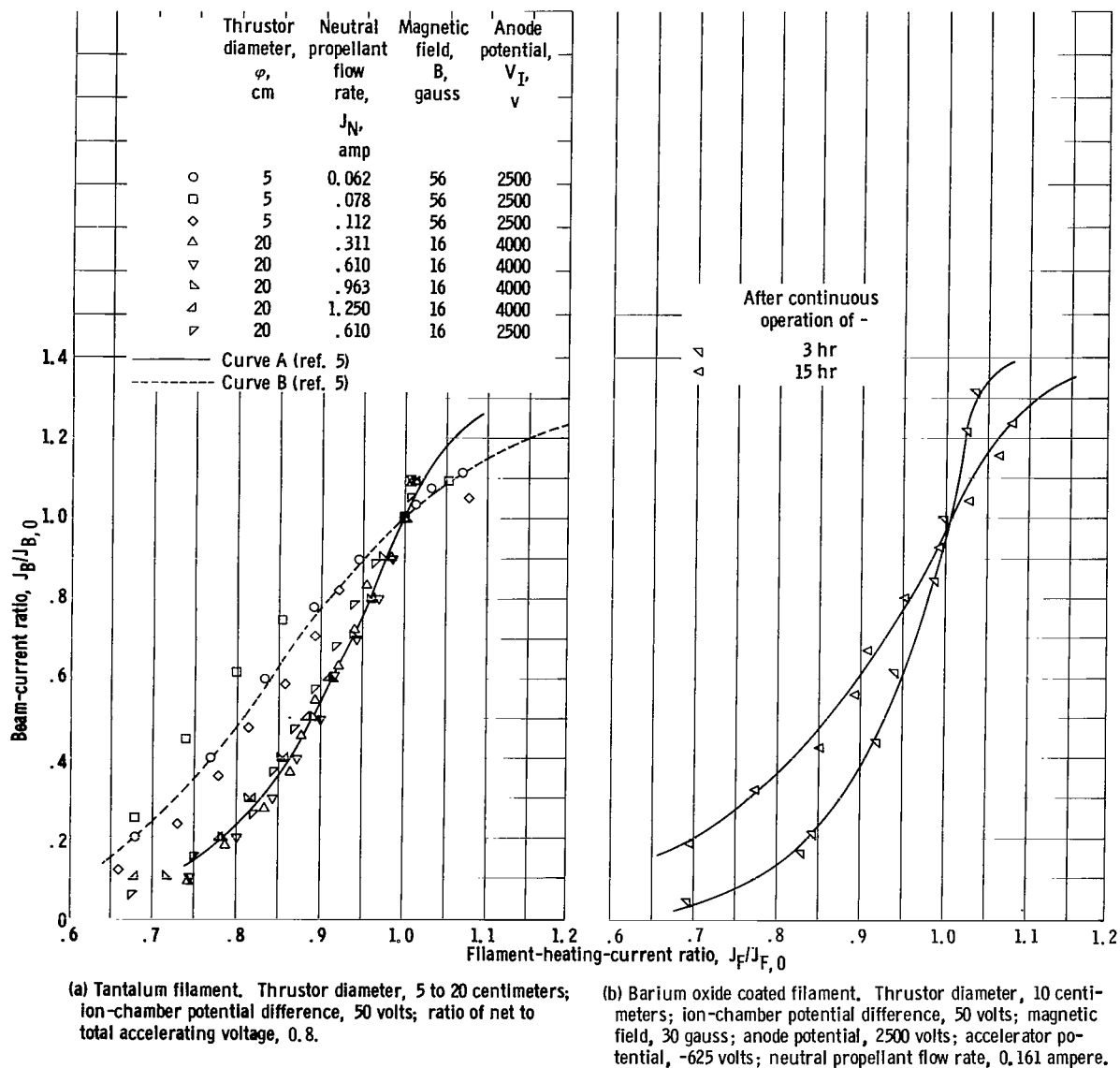


Figure 8. - Beam-current ratio as function of filament-heating-current ratio.

centimeter-diameter thrusters. The currents are expressed as a ratio or fraction of a base point value, where all base point values are the thruster operating values near a propellant utilization of 80 percent. Data are presented for a range of propellant flow rates for each size thruster. The data for the larger thruster for a range of propellant flow rates fell very close to those presented for a refractory metal filament used with the 10-centimeter-diameter thruster and reported in reference 5. The two curves in figure 8(a) are from this reference and represent two different refractory metal filaments that were used with the 10-centimeter-diameter unit. These two filaments are felt to represent an approximate range over which the characteristics of any given filament may vary. The variations in the filament heating characteristics were felt to be attributable to slight differences in the geometry of the filament

and ion chamber and to filament attrition rates. The data from the smallest thruster for three values of propellant flow rate could also be described by a curve from this reference, but a greater degree of scatter existed. Refractory metal filament characteristics and the variations with use are described more thoroughly in reference 11.

The 10-centimeter-diameter thruster was also operated with a barium oxide coated filament; these data are tabulated in table I(b). The results of the beam to filament current variations for this type cathode are presented in figure 8(b). The data were taken after 3 and 15 hours of continuous operation. The coated filament required a conditioning period during which the operation characteristics changed considerably. After conditioning, a plateau region is normally encountered, where a very gradual time variation in filament operation is present. The two curves presented in figure 8(b) were taken after the major portion of the filament conditioning had occurred. The data taken after 3 hours of operation are believed to represent the plateau region. The barium oxide coated filament presented herein is in an early stage of development, and the results may differ from a final version. On the basis of this preliminary investigation, however, the oxide cathode exhibits characteristics similar to those of the refractory filaments except that it was more sensitive near $J_F/J_{F,0} = 1$. The filament power required to maintain a given emission current was considerably lower than that required without the oxide coating. At values of filament heating current ratios above 1 a region of incipient instability existed. In this region localized filament heating seemed to occur as evidenced by pulsating hot spots, and an emission runaway condition seemed to

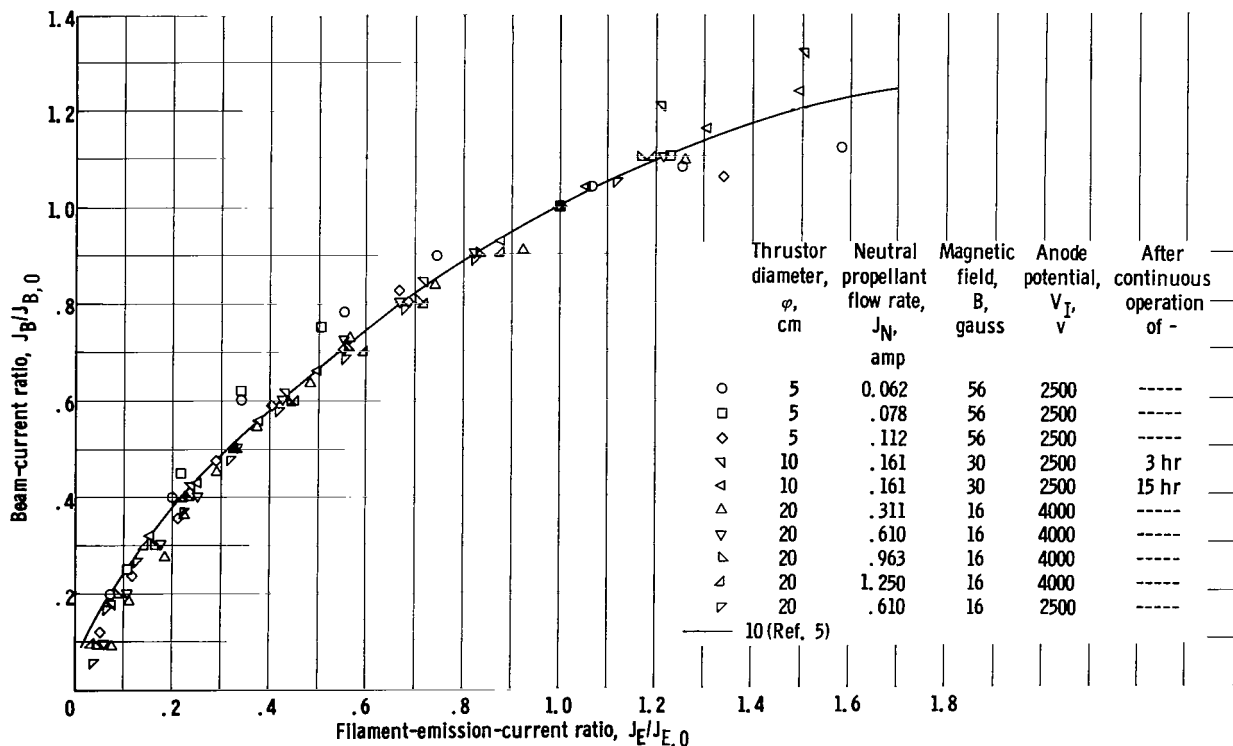


Figure 9. - Beam-current ratio as function of filament-emission-current ratio.

exist. The instability was principally a function of discharge chamber voltage and plasma chamber density.

The beam current ratios for various filament emission current ratios are shown in figure 9. All three thruster sizes and both refractory and oxide coated cathodes are included in this figure and are compared with the curve obtained for the 10-centimeter-diameter thruster in reference 5 for a wide range of operating conditions. The data for the three thruster sizes and a range of propellant flow rates, in general, fall quite close to the curve obtained for the 10-centimeter-diameter size. A relation exists between beam and emission current that is independent of thruster size and operating conditions. The largest deviation from this curve exists for the 5-centimeter-diameter thruster at propellant flow rates equivalent to 0.062 and 0.078 ampere. A departure from the curve can also be found for the coated cathode for emission current ratios greater than 1.

The filament heating current gains are presented in figure 10 as a function of filament heating current. These gains were graphically determined as in the Neutral Flow section for each of the curves in figure 8. The gains were also determined for the beam current to emission current data of figure 9 and are presented in figure 11. The emission current gains are relatively well defined by a single functional relation independent of filament characteristics or thruster size. The input to output relation, as determined through the ion chamber and accelerator section of the block design of figure 4 (p. 5), seems therefore to be the more significant. The emission current for a flight thruster would therefore be specified, and a control loop would be necessary to maintain this value by adjusting the inputs to the filament.

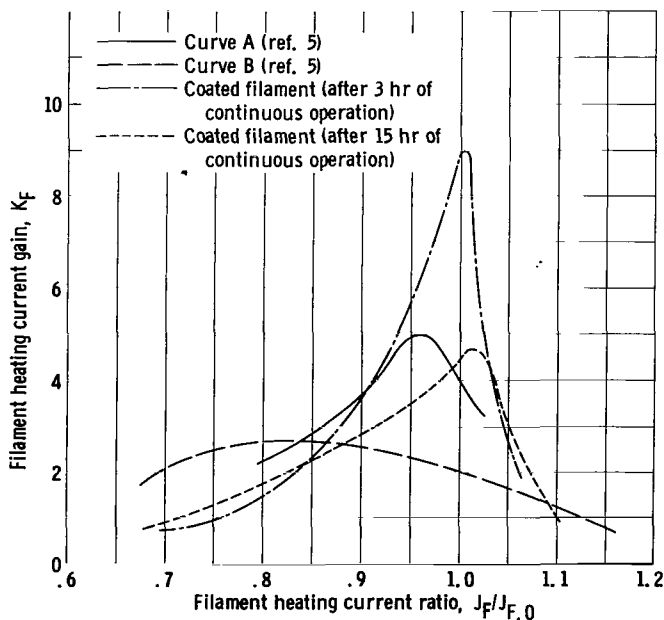


Figure 10. - Filament heating current gain as function of filament heating current.

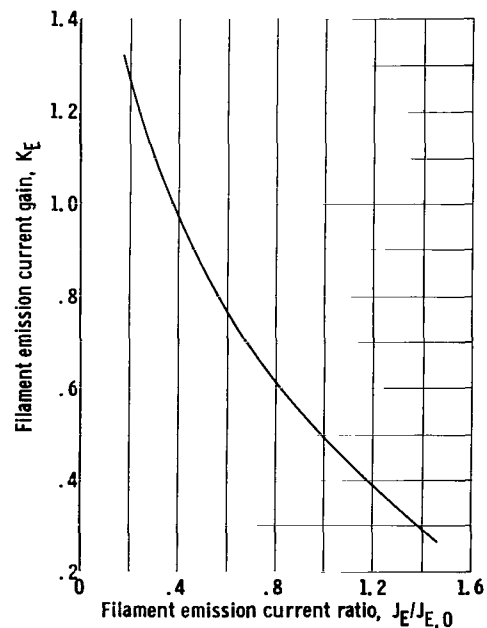


Figure 11. - Filament emission current gain as function of filament emission current ratio.

Anode Voltage (Net Accelerating Potential)

The beam current ratio as a function of anode voltage (net accelerating potential) is shown in figure 12 for the 5- and the 20-centimeter-diameter

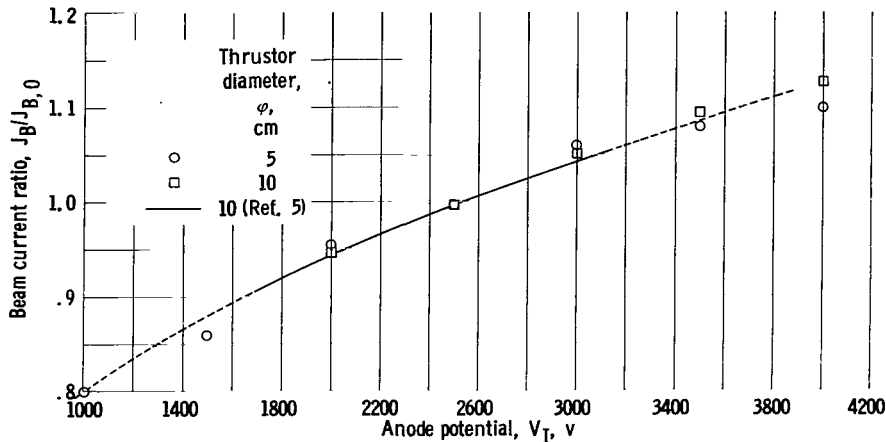


Figure 12. - Beam current ratio as function of anode potential for 5- to 20-centimeter-diameter thruster sizes. Ion-chamber potential difference, 50 volts; accelerator potential, -625 volts.

thrusters. (A curve for similar data obtained for the 10-centimeter size presented in ref. 5 is also shown in the figure.) The data were obtained at a constant filament heating current and accelerator potential. Magnetic field strength was held constant at the optimum value for each size thruster as described previously. All data were compared on the basis that the base point beam current is a value near a propellant utilization of 80 percent at an anode voltage of 2500 volts. Base point values of ion beam current used for comparison in this and in subsequent sections were 0.050 ampere for the 5-centimeter size (50 amp/m²) and 0.475 ampere for the 20-centimeter size (29.7 amp/m²). In the data from reference 5, a base point value of 0.125 ampere (31.3 amp/m²) was used. The results indicated that the input to output relation between anode voltage and ion beam is apparently independent of thruster size for the range of diameters

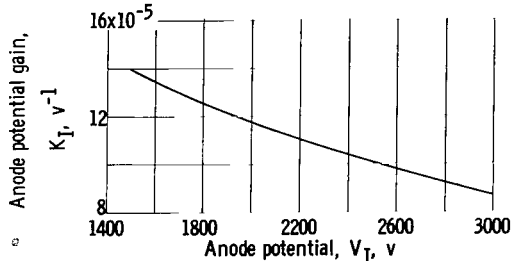


Figure 13. - Anode potential gain as function of anode potential.

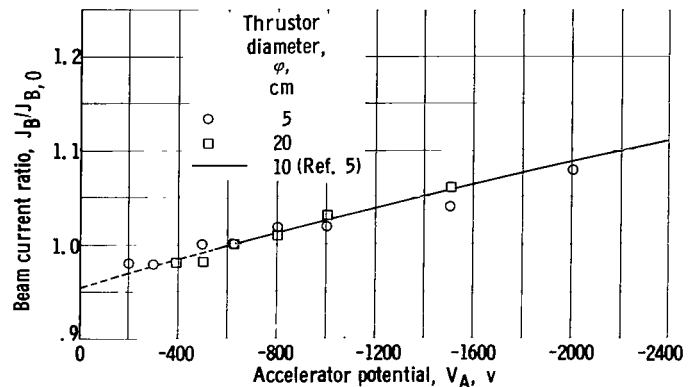


Figure 14. - Beam current ratio as function of accelerator potential for 5- to 20-centimeter-diameter thruster sizes. Ion-chamber potential difference, 50 volts; anode potential, 2500 volts.

considered. Steady-state gains determined for the 10-centimeter-diameter thruster would therefore be applicable for a 5- to 20-centimeter-diameter ion beam thruster. These gains are presented in figure 13.

Accelerator Voltage

The variation in beam current with accelerator potential is shown in figure 14. The faired curve again represents the 10-centimeter-diameter-thruster data from reference 5. The data for all three thruster sizes define a common curve within the experimental accuracy of the tests. The 5-centimeter-diameter-thruster data appears to define a curve with a slightly lower slope, hence a lower gain, but the resulting difference in beam current for accelerator voltage changes of the order of 500 volts is negligible. The accelerator potential gain K_A is presented in figure 15.

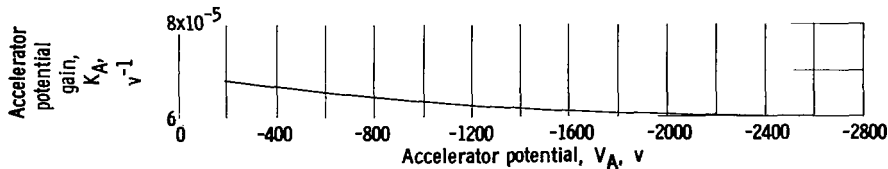


Figure 15. - Accelerator potential gain as function of accelerator potential.

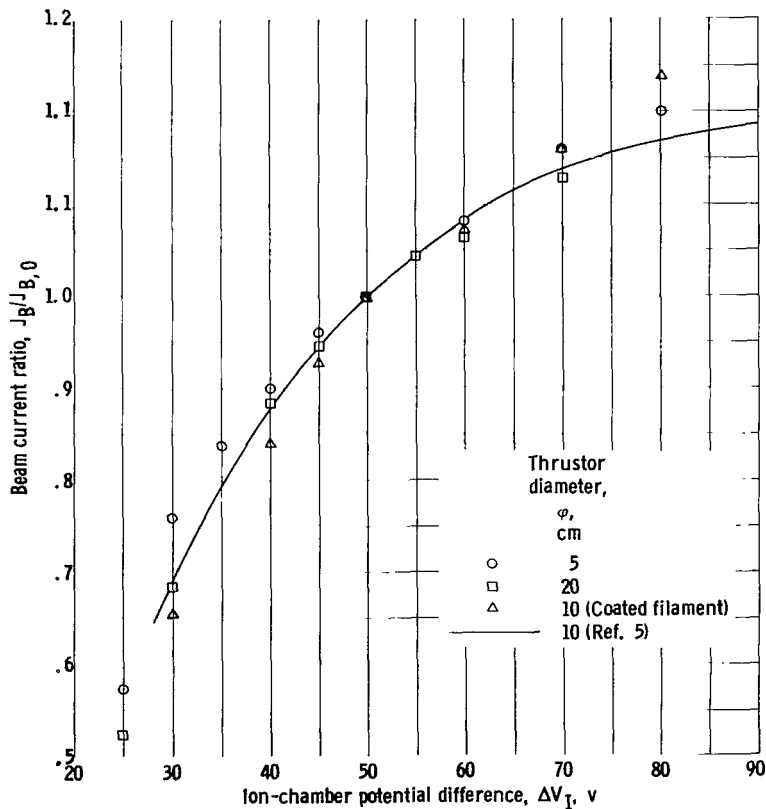


Figure 16. - Beam current ratio as function of ion-chamber potential difference for 5- to 20-centimeter-diameter thruster sizes. Anode potential, 2500 volts; accelerator potential, -625 volts.

Discharge Voltage (Ion-Chamber Potential Difference)

The effects of discharge voltage upon the beam current are shown in figure 16. In addition to data on variation of thruster size, the oxide coated cathode data obtained after 15 hours of thruster operation are also presented in the figure. In contrast to the effects found with anode voltage and accelerator voltage, the beam current data exhibited a wider spread as thruster size and type of filament was varied. The general trend of the data with discharge voltage, however, was similar for all sizes. At discharge voltages above 60 volts a slight upward trend in the beam current could be noted for both the 5-centimeter-diameter-thruster and the coated-filament data. At discharge voltages above 50 volts, the ion chamber operates with increased cathode heating by positive ion bombardment and increased multiple ionization of the mercury ions.

Both of these effects are in the direction of increasing the beam current. The increased bombardment is probably the more significant factor in the case of the coated cathode because the increased filament heating results in an increase in filament emission current.

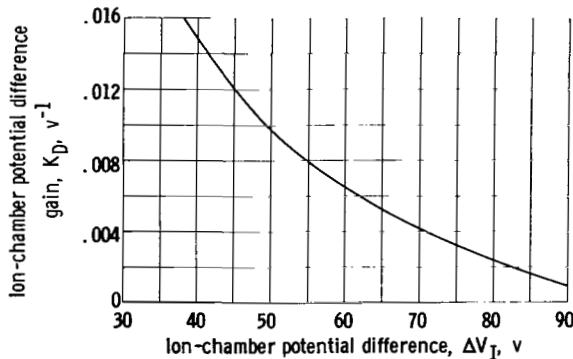


Figure 17. - Discharge voltage gain as function of discharge voltage.

The steady-state gains for the curve in figure 16 are presented in figure 17. These gain values K_D are felt to be representative of those that might be obtained over the range of thruster sizes considered. After suitable conditioning, coated cathodes also appear to exhibit characteristics similar to those of the refractory filaments.

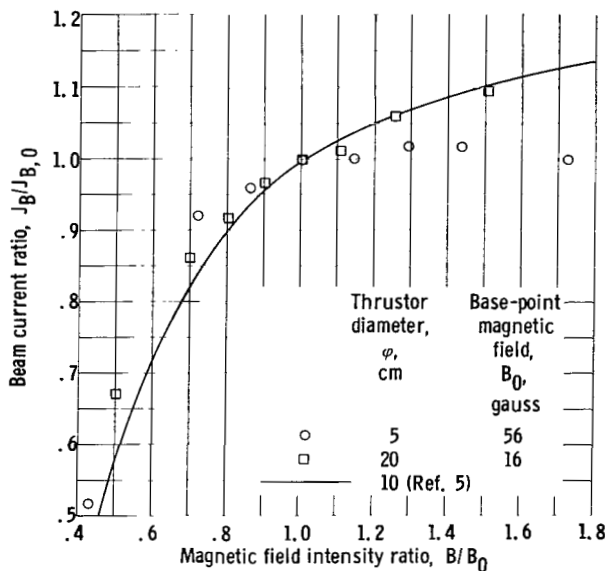


Figure 18. - Beam current ratio as function of magnetic field intensity ratio for 5- to 20-centimeter-diameter thruster sizes. Ion-chamber potential difference, 50 volts; anode potential, 2500 volts; accelerator potential, -625 volts.

Magnetic Field

The variation of beam current with magnetic field strength is shown in figure 18. The faired curve, representing the 10-centimeter-diameter thruster as before, and the data for the 20-centimeter-diameter thruster exhibited about the same variation in beam current both in trend and in magnitude. Because the magnetic field strength is scaled, the base-point field strength B_0 varied by a factor of 4 in inverse proportion to the thruster diameter. The base point beam current $J_{B,0}$ covered a range from 0.050 to 0.475 ampere. The only significant departure in the beam-

current - magnetic-field function was found with the 5-centimeter-diameter thruster at high field strengths. As discussed previously, one of the possible causes of poor ion-chamber performance with the 5-centimeter-diameter thruster is the energy dissipated in ohmic heating of the plasma. The ion-chamber radial potential difference as expressed by equation (5) is a function of the cyclotron radius, which is inversely proportional to the magnetic field

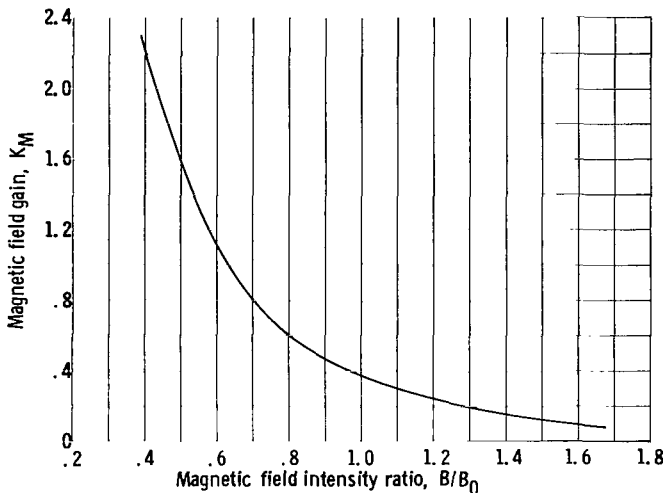


Figure 19. - Magnetic field gain as function of magnetic field intensity ratio.

strength. The energy dissipated in ohmic heating therefore varies as the square of the magnetic field strength. A rapidly increasing energy loss of this nature is thought to be one of the causes of the difference in beam current output at high field strengths for the smallest thruster. A study of the ion chamber (ref. 12) has also noted this effect in the 10-centimeter-diameter source at high magnetic fields.

The values of the magnetic field gain K_M were determined for the curve in figure 18 and are presented in figure 19.

CONCLUDING REMARKS

A program was undertaken to determine the effects of size on the process characteristics of an electron-bombardment ion thruster. The thruster characteristics and gains as presented in reference 5 for a 10-centimeter-diameter thruster were determined to be representative also of the 5- and the 20-centimeter-diameter thrusters with the exception of variations of beam current with neutral propellant flow. The greatest deviations existed for the smallest size unit, especially in the region of low neutral propellant flow rates.

The 10-centimeter-diameter thruster was also operated with a barium oxide coated filament in addition to the refractory metal cathodes normally employed. Process characteristics of the coated filament were somewhat time variant but, in general, were close to those of the refractory filaments. The functional relation of beam current ratio to emission current ratio, when determined about a base point of 80-percent propellant utilization, was independent of thruster size and type of filament used.

The similarity of output characteristics to the various input variables for thrusters covering a diameter range that varies by a factor of 4 permits a few broad generalizations. An increase in thruster size requires corresponding increases in input power supply ratings commensurate with the output beam power and thruster efficiency. The gain characteristics of the thruster itself are relatively independent of the thrust level. The only control system characteristics that may require modification in going from the smaller to the larger

|||| | ||||| |||

thruster sizes investigated therefore appear to be those associated with the characteristics of the input power supplies for space applications, which may change with beam power level.

These conclusions consider only the steady-state behavior of thruster operation and may not be rigorously correct where the characteristic time, which may be size dependent, becomes appreciable relative to the control system response times.

Lewis Research Center
National Aeronautics and Space Administration
Cleveland, Ohio, July 1, 1964

APPENDIX - SYMBOLS

B	magnetic field, gauss
\mathcal{E}	discharge chamber energy loss, ev/ion
F	thrust, newtons
g	gravitational constant, 9.8 m/sec ²
I	specific impulse, sec
J _A	accelerator impingement current, amp
J _B	ion beam current, amp
J _E	filament emission current, amp
J _F	filament heating current, amp
J _I	anode current, amp
J _M	magnetic field current, amp
J _N	neutral propellant flow rate, equivalent amp of Hg ⁺
J _{SD}	screen distributor current, amp
J ₋	electron current
K _A	accelerator voltage gain, $\partial(J_B/J_{B,0})/\partial V_A$, v ⁻¹
K _D	discharge voltage gain, $\partial(J_B/J_{B,0})/\partial(\Delta V_I)$, v ⁻¹
K _E	filament emission current gain, $\partial(J_B/J_{B,0})/\partial(J_E/J_{E,0})$
K _F	filament heating current gain, $\partial(J_B/J_{B,0})/\partial(J_F/J_{F,0})$
K _I	anode voltage gain, $\partial(J_B/J_{B,0})/\partial V_I$, v ⁻¹
K _M	magnetic field gain, $\partial(J_B/J_{B,0})/\partial(B/B_0)$
K _N	neutral flow gain, $\partial J_B/\partial J_N$, amp/equivalent amp
L _C	electron cyclotron radius
l	ion chamber length
m	mass flow rate, kg/sec
q/m	charge to mass ratio, 0.4811x10 ⁶ coulomb/kg for Hg ⁺

R	ratio of net to total accelerating voltage, $V_I/(V_I + V_A)$
V_A	accelerator potential (with respect to ground), v
V_I	anode or net accelerating potential (with respect to ground), v
\bar{V}_-	electron thermal potential
ΔV_F	filament potential difference, v
ΔV_I	ion-chamber potential difference (discharge voltage), v
ΔV_M	magnetic field potential difference, v
ΔV_r	discharge chamber radial potential variation, v
\bar{v}	average velocity, m/sec
x	arbitrary input variable
η_u	propellant utilization efficiency, J_B/J_N
η_-	electron density
ϕ	thruster diameter, cm
σ_E	effective cross section
Subscript:	
0	design or base point

REFERENCES

1. Kaufman, H. R., and Reader, P. D.: Experimental Performance of an Ion Rocket Employing an Electron-Bombardment Ion Source. Progress in Astronautics and Rocketry. Vol. 5 - Electrostatic Propulsion. Academic Press, 1960, p. 3.
2. Reader, Paul D.: Investigation of 10-Centimeter-Diameter Electron-Bombardment Ion Rocket. NASA TN D-1163, 1962.
3. Kerslake, William R., and Pawlik, Eugene V.: Additional Studies of Screen and Accelerator Grids for Electron-Bombardment Ion Thrusters. NASA TN D-1411, 1963.
4. Gille, J. C., Pélegrin, M. J., and Decaulne, P.: Feedback Control Systems. McGraw-Hill Book Co., Inc., 1959.
5. Nakanishi, Shigeo, Pawlik, Eugene V., and Baur, Charles W.: Experimental Evaluation of Steady-State Control Properties of an Electron-Bombardment Ion Thruster. NASA TN D-2171, 1964.
6. Reader, Paul D.: Scale Effects on Ion Rocket Performance. ARS Jour., vol. 32, no. 5, May 1962, pp. 711-714.
7. Milder, Nelson L.: Comparative Measurements of Singly and Doubly Ionized Mercury Produced by Electron-Bombardment Ion Engine. NASA TN D-1219, 1962.
8. Kaufman, Harold R.: The Neutralization of Ion-Rocket Beams. NASA TN D-1055, 1961.
9. Mickelsen, William R., and Kaufman, Harold R.: Electrostatic Thrusters for Space Propulsion, Present and Future. Paper Presented at British Interplanetary Soc. Symposium on Advanced Prop. Systems, London (England), Oct. 9, 1963.
10. Kaufman, Harold R.: An Ion Rocket With an Electron-Bombardment Ion Source. NASA TN D-585, 1961.
11. Milder, N. L., and Kerslake, W. R.: Evaluation of Filament Deterioration in Electron-Bombardment Ion Sources. NASA TN D-2173, 1964.
12. Domitz, Stanley: Experimental Evaluation of a Direct-Current Low-Pressure Plasma Source. NASA TN D-1659, 1963.

TABLE I. - THRUSTOR PERFORMANCE

(a) 5-Centimeter-diameter thruster

Anode potential, V_I , v	Accelerator potential, V_A , v	Ion-chamber potential difference, ΔV_I , v	Beam current, J_B , amp	Anode current, J_I , amp	Filament emission current, J_E , amp	Filament heating current, J_F , amp	Neutral propellant flow rate, J_N , equivalent amp	Magnetic field at screen, B_0 , gauss	Ratio of net to total accelerating voltage, $R = \frac{V_I}{V_I + V_A }$
2500	-625	50	0.002	0.10	0.10	9.0	0.029	56	0.800
			.004	.19	.20	9.9			
			.006	.60	.62	13.0			
			.007	.60	.69	13.5			
			0.005	0.12	0.10	9.5	0.041	56	0.800
			.010	.25	.20	10.2			
			.012	.30	.29	10.9			
			.015	.47	.41	11.1			
			.020	.84	.84	12.2			
			.022	1.02	1.09	13.0			
			.025	1.40	1.50	14.0			
			.026	1.50	1.60	14.9			
			0.010	0.20	0.11	8.8	0.062	56	0.800
			.020	.31	.30	10.0			
			.030	.59	.51	10.8			
			.039	.89	.83	11.6			
			.045	1.13	1.12	12.3			
			.050	1.50	1.50	13.0			
			.052	1.59	1.60	13.3			
			.054	1.82	1.90	13.8			
			.056	2.22	2.38	14.8			
			.060	3.29	3.50	17.2			
			0.006	0.10	0.09	7.5	0.078	56	0.800
			.015	.21	.19	8.8			
			.027	.40	.39	9.6			
			.037	.69	.61	10.4			
			.045	.98	.90	11.1			
			.060	1.75	1.79	13.0			
			.066	2.09	2.20	13.7			
			0.010	0.15	0.10	9.2	0.112	56	0.800
			.020	.29	.21	10.2			
			.030	.48	.38	10.8			
			.040	.70	.52	11.4			
			.050	.92	.72	12.0			
			.060	1.20	.99	12.5			
			.070	1.50	1.20	12.9			
			.085	2.22	1.79	14.0			
			.090	2.90	2.40	15.1			
	-200	50	0.049	1.55	1.60	13.0	0.062	56	0.926
	-300		.049	1.58	1.60				.893
	-500		.050	1.55	1.50				.833
	-625		.050	1.50	1.50				.800
	-800		.051	1.55	1.59				.758
	-1000		.051	1.51	1.50				.714
	-1500		.052	1.50	1.50				.625
	-2000		.054	1.50	1.50				.556

TABLE I. - Continued. THRUSTOR PERFORMANCE

(a) Concluded. 5-Centimeter-diameter thrustor

Anode potential, V_I , v	Accelerator potential, V_A , v	Ion-chamber potential difference, ΔV_I , v	Beam current, J_B , amp	Anode current, J_I , amp	Filament emission current, J_E , amp	Filament heating current, J_F , amp	Neutral propellant flow rate, J_N , equivalent amp	Magnetic field at screen, B_0 , gauss	Ratio of net to total accelerating voltage, $R = \frac{V_I}{V_I + V_A }$
1000	-625	50	0.040	1.62	1.63	13.0	0.062	56	0.615
1500			.043	1.58	1.60				.706
2000			.048	1.55	1.60				.762
2500			.050	1.55	1.59				.800
3000			.053	1.55	1.58				.828
3500			.054	1.55	1.55				.849
4000			.055	1.55	1.54				.865
4500			.057	1.51	1.51				.878
2500	-625	25	0.029	1.30	1.30	13.0	0.062	56	0.800
		30	.038	1.45	1.43				
		35	.042	1.52	1.53				
		40	.045	1.60	1.62				
		45	.048	1.63	1.70				
		50	.050	1.70	1.75				
		60	.054	1.80	1.88				
		70	.058	1.82	1.90				
		80	.060	1.91	2.00				
		50	0.002	0.16	0.15	13.0	0.062	16	0.800
			.026	1.54	1.77			22	
			.046	1.84	1.80			37	
			.048	1.82	1.80			45	
			.050	1.80	1.82			52	
			.050	1.80	1.82			59	
			.051	1.75	1.79			67	
			.051	1.67	1.73			74	
			.050	1.59	1.63			89	
			.048	1.54	1.56			104	
			.047	1.49	1.52			119	
			.045	1.35	1.41			148	

(b) 10-Centimeter-diameter thrustor








2500	-625	50	0.005	0.09	0.04	14.0	0.161	30	0.800	
			.020	.12	.10	17.6				
			.026	.20	.12	17.9				
			.053	.50	.40	19.5				
			.077	.90	.71	20.0				
			.106	1.40	1.19	21.0				
			.125	2.02	1.65	21.2				
			.153	2.55	2.00	21.8				
			.165	3.10	2.50	22.0				
			20	0.045	1.12	1.00				21.2
			30	.082	1.58	1.30				
			40	.105	1.77	1.51				
			45	.116	1.86	1.51				
			50	.125	1.98	1.62				
			60	.134	2.10	1.65				
			70	.145	2.30	1.78				
			80	.155	2.55	1.90				
			90	.160	2.78	2.00				

TABLE I. - Continued. THRUSTOR PERFORMANCE

(b) Concluded. 10-Centimeter-diameter thrustor

Anode potential, V_I , v	Accelerator potential, V_A , v	Ion-chamber potential difference, ΔV_I , v	Beam current, J_B , amp	Anode current, J_I , amp	Filament emission current, J_E , amp	Filament heating current, J_F , amp	Neutral propellant flow rate, J_N , equivalent amp	Magnetic field at screen, B_0 , gauss	Ratio of net to total accelerating voltage, $R = \frac{V_I}{V_I + V_A }$
2500	-625	50	0.023	0.21	0.12	15.5	0.161	30	0.800
			.040	.32	.25	17.2			
			.053	.59	.41	18.9			
			.070	.82	.61	19.9			
			.083	1.10	.81	20.2			
			.100	1.40	1.10	21.2			
			.116	1.78	1.42	22.1			
			.125	1.99	1.60	22.2			
			.130	2.10	1.70	22.9			
			.145	2.52	2.10	23.7			
			.155	2.89	2.40	24.0			

(c) 20-Centimeter-diameter thrustor

4000	-1000	50	0.025	0.2	0.2	24.5	0.311	16	0.800
			.050	.4	.3	26.0			
			.075	.6	.5	27.5			
			.100	.8	.6	28.5			
			.125	1.0	.8	29.0			
			.150	1.3	1.0	29.5			
			.175	1.6	1.3	30.5			
			.200	2.0	1.5	31.0			
			.230	2.5	2.0	31.5			
			.250	2.7	2.3	32.5			
			.275	3.4	2.7	33.0			
			.300	4.1	3.4	33.5			
			0.050	0.4	0.3	26.0	0.610	16	0.800
			.100	.8	.6	28.0			
			.150	1.3	1.0	29.5			
			.200	1.9	1.4	30.5			
			.250	2.5	1.9	31.5			
			.300	3.3	2.4	32.0			
			.350	4.2	3.1	33.0			
			.400	5.1	3.8	34.0			
			.450	6.2	4.6	34.5			
			.500	7.5	5.6	35.0			
			.550	8.9	6.8	35.5			
			0.075	0.5	0.4	26.5	0.963	16	0.800
			.150	1.2	0.8	28.5			
			.225	2.0	1.4	30.0			
			.300	3.0	2.1	31.5			
			.375	4.3	3.0	33.0			
			.450	5.6	4.0	34.0			
			.527	7.2	5.1	35.0			
			.600	8.7	6.4	35.5			
			.675	10.2	7.5	36.0			
			.750	12.1	9.0	37.0			
			.825	14.1	10.4	38.0			

TABLE I. - Concluded. THRUSTOR PERFORMANCE

(c) Concluded. 20-Centimeter-diameter thrustor

Anode poten- tial, V_I , v	Accel- erator potential, V_A , v	Ion- chamber potential difference, ΔV_I , v	Beam current, J_B , amp	Anode current, J_I , amp	Filament emission current, J_E , amp	Filament heating current, J_F , amp	Neutral propellant flow rate, J_N , equivalent amp	Magnetic field at screen, B_0 , gauss	Ratio of net to total accelerating voltage, $R = \frac{V_I}{V_I + V_A }$
4000	-1000	50	0.100	0.5	0.4	26.0	1.250	16	0.800
			.200	1.3	.9	29.0			
			.300	2.5	1.7	31.5			
			.400	3.9	2.7	33.0			
			.500	5.5	3.9	34.0			
			.600	7.5	5.3	35.0			
			.700	9.6	7.0	36.0			
			.800	11.5	8.4	37.0			
			.900	13.9	10.3	38.0			
			1.000	16.0	11.7	38.5			
			1.100	19.2	14.0	39.5			
2500	-625	50	0.025	0.25	0.2	28.0	0.610	16	0.800
			.075	.6	.4	31.5			
			.125	1.2	.8	34.0			
			.175	1.9	1.4	35.0			
			.225	2.8	2.0	36.0			
			.275	3.6	2.6	37.0			
			.325	4.8	3.5	38.0			
			.375	5.8	4.3	39.0			
			.425	7.1	5.2	40.0			
			.475	8.4	6.3	41.5			
			.500	9.4	7.1	42.0			
		50	0.465	8.4	6.3	41.5	0.610	16	0.852
			.465	8.4	6.25				.833
			.475	8.45	6.25				.800
			.480	8.5	6.35				.758
			.490	8.5	6.35				.714
			.505	8.6	6.45				.625
2000	-625	50	0.450	8.2	6.15	41.5	0.610	16	0.762
2500			.475	8.4	6.25				.800
3000			.500	8.0	6.0				.828
3500			.520	8.0	5.95				.848
4000			.535	7.8	5.75				.865
2500	-625	25	0.250	5.15	4.8	41.5	0.610	16	0.800
			.325	5.98	5.4				
			.420	7.25	5.9				
			.450	7.8	6.05				
			.475	8.18	6.10				
			.495	8.85	6.30				
			.505	9.1	6.40				
			.535	10.1	6.6				
		50	0.124	4.9	4.5	41.5	0.610	4.0	0.800
			.320	7.5	5.8			8.0	
			.405	7.95	6.0			11.2	
			.435	7.95	5.95			12.8	
			.460	8.18	6.1			14.4	
			.475	8.2	6.1			16.0	
			.480	8.25	6.2			17.6	
			.500	8.4	6.35			20.0	
			.520	8.4	6.4			24.0	

2/7/25
22

"The aeronautical and space activities of the United States shall be conducted so as to contribute . . . to the expansion of human knowledge of phenomena in the atmosphere and space. The Administration shall provide for the widest practicable and appropriate dissemination of information concerning its activities and the results thereof."

—NATIONAL AERONAUTICS AND SPACE ACT OF 1958

NASA SCIENTIFIC AND TECHNICAL PUBLICATIONS

TECHNICAL REPORTS: Scientific and technical information considered important, complete, and a lasting contribution to existing knowledge.

TECHNICAL NOTES: Information less broad in scope but nevertheless of importance as a contribution to existing knowledge.

TECHNICAL MEMORANDUMS: Information receiving limited distribution because of preliminary data, security classification, or other reasons.

CONTRACTOR REPORTS: Technical information generated in connection with a NASA contract or grant and released under NASA auspices.

TECHNICAL TRANSLATIONS: Information published in a foreign language considered to merit NASA distribution in English.

TECHNICAL REPRINTS: Information derived from NASA activities and initially published in the form of journal articles.

SPECIAL PUBLICATIONS: Information derived from or of value to NASA activities but not necessarily reporting the results of individual NASA-programmed scientific efforts. Publications include conference proceedings, monographs, data compilations, handbooks, sourcebooks, and special bibliographies.

Details on the availability of these publications may be obtained from:

SCIENTIFIC AND TECHNICAL INFORMATION DIVISION
NATIONAL AERONAUTICS AND SPACE ADMINISTRATION
Washington, D.C. 20546